ChemComm

COMMUNICATION

View Article Online
View Journal | View Issue

Cite this: *Chem. Commun.*, 2016, 52, 7273

Received 9th March 2016,
Accepted 5th May 2016

DOI: 10.1039/c6cc02086k

www.rsc.org/chemcomm

Observation of phase-retention behavior of the $HC(NH_2)_2PbI_3$ black perovskite polymorph upon mesoporous TiO_2 scaffolds†

Yuanyuan Zhou,*[a] Joonsuh Kwun,[a] Hector F. Garces,[a] Shuping Pang*[b] and Nitin P. Padture*[a]

The α → δ phase transition, which occurs favorably in planar films of a black α-$HC(NH_2)_2PbI_3$ (α-$FAPbI_3$) perovskite in the amibent, is retarded when α-$FAPbI_3$ is deposited upon mesoporous TiO_2 scaffolds. It is hypothesized that this is due to the synergistic effect of the partial encapsulation of α-$FAPbI_3$ by the mesoporous TiO_2 and the elevated activation energy for the transition reaction associated with the substantial increase of the TiO_2/α-$FAPbI_3$ interfacial area in the mesoscopic system.

Formamidinium lead triiodide ($HC(NH_2)_2PbI_3$ or $FAPbI_3$) perovskite has been attracting increasing attention in the field of perovskite solar cells (PSCs) due to its broader light absorption compared to the widely studied methylammonium lead triiodide ($CH_3NH_3PbI_3$ or $MAPbI_3$).[1–4] In addition, the $FAPbI_3$ perovskite has shown superior thermal stability,[3] which has important implications for the practical deployment of PSCs. While these two important attributes of the $FAPbI_3$ perovskite have been discussed in the early stages of the development of this perovskite, its poor ambient stability has become a significant concern recently.[4,5] In fact, $FAPbI_3$ has two distinct polymorphs at ambient temperature:[6] (i) the perovskite phase (α-$FAPbI_3$, space group $P3m1$[6] or $Pm\bar{3}m$[7]), which appears 'black' with a direct bandgap of ~1.45 eV and (ii) the non-perovskite phase (δ-$FAPbI_3$, space group $P6_3mc$[6]), which is 'yellow' with an indirect bandgap of ~2.48 eV. Stoumpos *et al.*[6] and Jeon *et al.*[8] have shown that pure α-$FAPbI_3$ perovskite powders transform rapidly to δ-$FAPbI_3$ when exposed to ambient conditions, and a similar phenomenon was also reported by Li *et al.*[5] in the case of planar thin films. (This is reminiscent of the polymorphic $CsSnI_3$.[9]) In this context, the retention of the α-$FAPbI_3$ perovskite phase is critical for its function in the solar cells because δ-$FAPbI_3$, the degradation product, is not a good light absorber.[5] Here, we report the discovery of the phase-retention behavior of the α-$FAPbI_3$ perovskite upon mesoporous TiO_2 scaffolds (MTS) under ambient conditions, which is hypothesized to be a synergistic effect of the partial encapsulation of α-$FAPbI_3$ by TiO_2 and the elevated activation energy associated with the α-$FAPbI_3$ perovskite in contact with the high-surface-area MTS.

Fig. 1A shows the evolution of the X-ray diffraction (XRD) patterns of a phase-pure α-$FAPbI_3$ perovskite thin film without (planar) and with MTS upon exposure to the ambient (room temperature (RT), 45 ± 5% relative humidity). The α-$FAPbI_3$ perovskite thin films are of the same thickness in both cases, deposited using a method reported elsewhere[10] and described in the ESI.† (Note that the higher relative humidity was chosen to accelerate the α-$FAPbI_3$ degradation.) It is clear that the planar α-$FAPbI_3$ perovskite thin film degrades very rapidly with substantial formation of the δ-$FAPbI_3$ phase in 24 h, which results in the obvious reduction in light absorption across the entire wavelength range, from UV to near-IR. The film is nearly bleached, as seen in the inset in Fig. 1B. In the case of the α-$FAPbI_3$ film deposited upon MTS, no obvious phase transition is detected in 4 h (Fig. 1C), and only a weak 001 δ-$FAPbI_3$

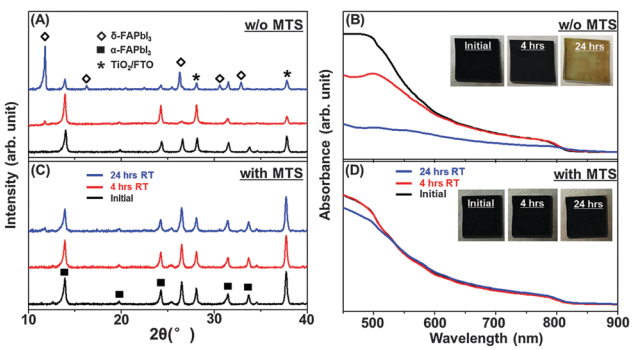

Fig. 1 Evolution of XRD patterns and UV-vis spectra of phase-pure α-$FAPbI_3$ perovskite thin films before and after exposure to the ambient (RT, 45 ± 5% relative humidity): (A and B) without MTS (planar) and (C and D) with MTS. Insets in (B) and (D) are corresponding to optical photographs of the thin films.

[a] *School of Engineering, Brown University, Providence, RI 02912, USA. E-mail: yuanyuan_zhou@brown.edu, nitin_padture@brown.edu*

[b] *Qingdao Institute of Bioenergy and Bioprocess Technology, Chinese Academy of Sciences, Qingdao 266101, P. R. China. E-mail: pangsp@qibet.ac.cn*

† Electronic supplementary information (ESI) available: Experimental details. See DOI: 10.1039/c6cc02086k

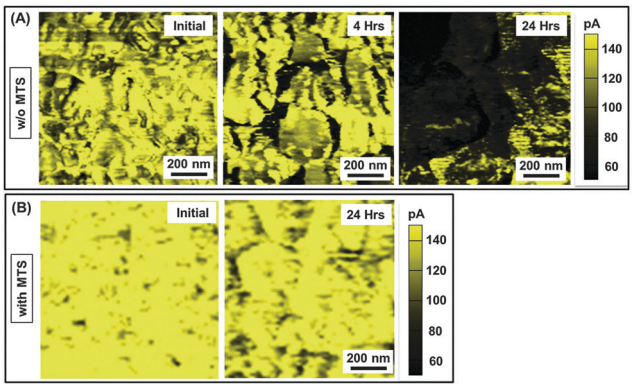

Fig. 2 Conductive AFM maps of α-$FAPbI_3$ perovskite thin film as a function of ambient-exposure time: (A) without MTS (planar) and (B) with MTS.

peak evolves after 24 h exposure to the ambient. Correspondingly, the film still appears black, and the optical absorption of the perovskite film is essentially retained (Fig. 1D). These results indicate clearly that the ambient stability of the α-$FAPbI_3$ perovskite thin film is significantly improved when MTS is present.

Fig. 2 shows conductive-AFM maps of the surface of the α-$FAPbI_3$ perovskite thin film without MTS (planar) and with MTS (capping layer). Initially, both films exhibit uniform conductivity at the nanoscale, indicative of continuous phase-purity of the perovskite in the film. After 24 h exposure to the ambient, the surface of the planar perovskite film loses its conductivity significantly. However, the surface conductivity is retained in the presence of the MTS. The retention of the conductivity in the latter is attributed to the lack of phase transition, since the electrical conductivity of α-$FAPbI_3$ (1.1×10^{-7} Ω^{-1} cm^{-1}) is significantly higher than that of δ-$FAPbI_3$ (8.9×10^{-9} Ω^{-1} cm^{-1}).[11] These results indicate that the surface of the α-$FAPbI_3$ perovskite thin film is also more stable under ambient conditions in the presence of the MTS.

To understand the origin of the enhanced ambient stability with MTS, the crystal morphologies of both perovskite thin films are studied using scanning electron microscopy (SEM) and XRD. Fig. 3A and B show typical cross-sectional morphologies of an α-$FAPbI_3$ perovskite thin film with and without the MTS, respectively. The overall thickness of the perovskite-containing layer is ~400 nm in both cases. In the planar thin film, the α-$FAPbI_3$ phase consists of an uniform layer over the substrate, as seen in Fig. 3A. High-resolution XRD analysis in Fig. 3C shows a characteristic 002 peak (indexed according to the suggested $Pm\bar{3}m$ symmetry[7]) of the α-$FAPbI_3$ perovskite, which can be fitted as a single peak at 24.3° (0.2° FWHM). However, for the film with the MTS, the ~400 nm α-$FAPbI_3$ perovskite layer is composed of two sub-layers as seen in Fig. 3B: a capping layer and a mesostructured layer comprising a nanocomposite of perovskite and TiO_2 nanoparticles. As a result, in Fig. 3D, the 002 peak of the α-$FAPbI_3$ perovskite is fitted with two components: a sharp peak at 24.3° (0.2° FWHM) and a broad fit peak at 24.1° (0.5° FWHM). This indicates that two distinct types of perovskite grain morphologies exist in the α-$FAPbI_3$ perovskite film that is deposited upon MTS, which is similar to the $MAPbI_3$ perovskite in our earlier studies.[12]

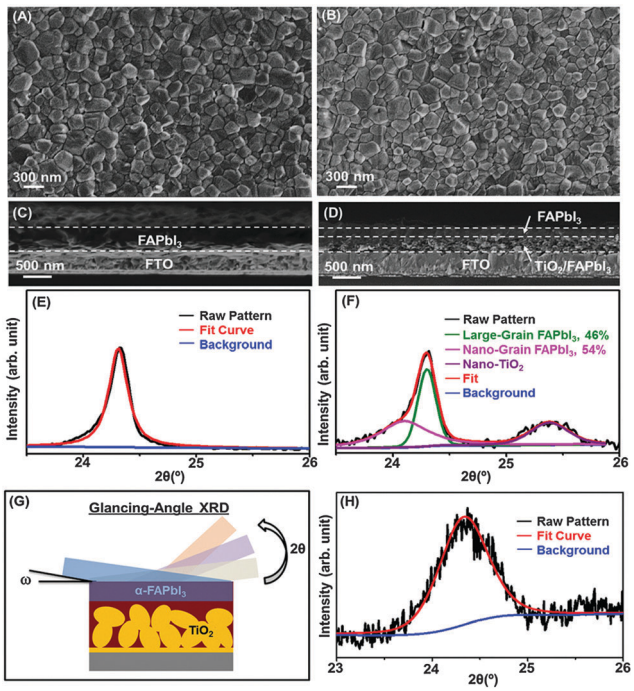

Fig. 3 Top-view and cross-sectional SEM images of α-$FAPbI_3$ perovskite thin films: (A and C) without MTS (planar) and (B and D) with MTS. XRD patterns and fits of the α-$FAPbI_3$ perovskite thin films: (E) without MTS (planar) and (F) with MTS. (G) Schematic illustration of glancing-angle XRD and (H) corresponding XRD pattern and fit of the α-$FAPbI_3$ perovskite thin film with MTS.

Using the Scherrer equation, the grain size corresponding to the broad peak is estimated at ~20 nm, which is about the size of the mesopores within the MTS. While the sizes of the grains in the capping layer and the planar thin film may be beyond the validity of the application of the Scherrer equation, the in-plane grain sizes are estimated to be ~250 nm in both cases from the SEM images. To confirm further the above argument, glancing-incident XRD experiments were conducted, where the X-ray beam is incident on the sample at a very small angle of $\omega = 0.7°$. This allows the characterization of only the capping perovskite layer, as illustrated in Fig. 3G. The resultant XRD pattern in Fig. 3H excludes the peaks of the mesostructured perovskite/MTS nanocomposite layer, and correspondingly shows a symmetric diffraction peak at 24.3°, which is consistent with the above XRD analysis.

It is now clear that the MTS has created a three-dimensional (3-D) constraint for solution crystallization of the α-$FAPbI_3$ perovskite, where nano-sized perovskite grains form within the MTS, compared to the coarse perovskite grains on the less-constrained free surface.[12] These nano-grains (consisting of ~46% of the perovskite phase upon MTS) are essentially encapsulated within the ceramic TiO_2 mesopores and as such are protected from the ambient atmosphere and stabilized, which is to be expected. Interestingly, the conductive AFM results show that the α → δ phase transition in the $FAPbI_3$ capping layer is also retarded, although the interaction of the top surfaces in both the α-$FAPbI_3$ perovskite capping layer and

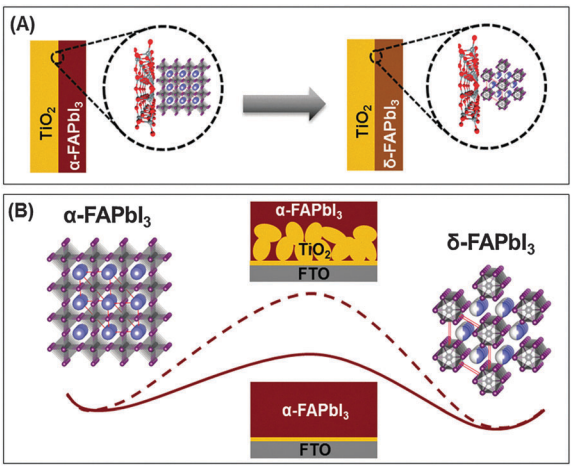

Fig. 4 Schematic illustrations: (A) highlighting the difference in the interface characteristics of α-$FAPbI_3$/TiO2 and δ-$FAPbI_3$/TiO_2 interfaces and (B) depicting the increase of the energy barrier for the α-$FAPbI_3$ → δ-$FAPbI_3$ transformation with an increase in the $FAPbI_3$/TiO_2 interfacial area.

the planar thin film with an ambient atmosphere occurs in a similar manner (Fig. 3A and B). This could be due to the fact that the MTS incorporation also increases the activation energy for the α-$FAPbI_3$ → δ-$FAPbI_3$ transition. As illustrated in Fig. 4A, when the α → δ transition occurs on the TiO_2 substrate, the possible interfacial bonds between α-$FAPbI_3$ and TiO_2 have to be broken in order to build new interfaces between δ-$FAPbI_3$ and TiO_2, which could add to the energy barrier for the transition. This is supported by the fact that the planar α-$FAPbI_3$ thin film appears to be more stable than the α-$FAPbI_3$ free-standing particles. In the case of MTS, a 3-D TiO_2 surface that interacts with α-$FAPbI_3$ is created. Typically, a mesoporous TiO_2 layer with an average pore size of ~20 nm has a surface area of ~55 m^2 g^{-1} and a porosity of 50% (TiO_2 density is 4.25 g cm^{-3}).[13] In this study, the thickness of such a mesoporous TiO_2 layer is ~250 nm. From a simple calculation, the TiO_2 surface area of the MTS is found to be ~29 m^2 per m^2 of the substrate. In other words, the TiO_2/α-$FAPbI_3$ interface area in the film with MTS is about 30 times that in the planar film. Such a large increase in interface area will correspondingly lead to an obvious increase of activation energy for the α → δ transition as illustrated in Fig. 4B. In this hypothesis, the α-$FAPbI_3$ phase in the mesopores and the capping layer in fact form a continuous structure interacting with TiO_2 and are thus considered as a whole. Fig. S2 (ESI†) plots the retention of the film absorption as a function of the MTS thickness (with constant total perovskite thickness). These results confirm that the α → δ transition becomes more retarded with an increase of MTS thickness (or TiO_2/α-$FAPbI_3$ interfacial area) and support this hypothesis.

In conclusion, we report the discovery that the transformation of the α-$FAPbI_3$ perovskite to the δ-$FAPbI_3$ non-perovskite under ambient conditions is significantly retarded upon the MTS. This behavior is related to the 3-D encapsulation of part of the perovskite in the TiO_2 mesopores, and the increased energy barrier for the α → δ transition owing to the high contact area between the perovskite and TiO_2. A similar effect is observed when an Al_2O_3 mesoporous scaffold is used instead of MTS (Fig. S2 in ESI†), where similar mechanisms may be at play. These results imply that a high-surface-area mesoporous scaffold can be key to the ambient stability of the pure α-$FAPbI_3$, and this concept could be extended to other polymorphic materials such as $CsSnI_3$.

Financial support for this work from the U.S. National Science Foundation (DMR 1305913, OIA-1538893) and the International S&T Cooperation Program of China (2015DFG62670) is gratefully acknowledged.

Notes and references

1 S. D. Stranks and H. J. Snaith, *Nat. Nanotechnol.*, 2015, **10**, 391–402; W. S. Yang, J. H. Noh, N. J. Jeon, Y. C. Kim, S. Ryu, J. Seo and S. I. Seok, *Science*, 2015, **348**, 1234–1237.
2 (*a*) S. Pang, H. Hu, J. Zhang, S. Lv, Y. Yu, F. Wei, T. Qin, H. Xu, Z. Liu and G. Cui, *Chem. Mater.*, 2014, **26**, 1485–1491; (*b*) T. M. Koh, K. Fu, Y. Fang, S. Chen, T. C. Sum, N. Mathews, S. G. Mhaisalkar, P. P. Boix and T. Baikie, *J. Phys. Chem. C*, 2014, **118**, 16458–16462; (*c*) J.-W. Lee, D.-J. Seol, A.-N. Cho and N.-G. Park, *Adv. Mater.*, 2014, **26**, 4991–4998; (*d*) Y. Zhou and K. Zhu, *ACS Energy Lett.*, 2016, **1**, 64–66; (*e*) S. Lv, S. Pang, Y. Zhou, N. P. Padture, H. Hu, L. Wang, X. Zhou, H. Zhu, L. Zhang, C. Huang and G. Cui, *Phys. Chem. Chem. Phys.*, 2014, **16**, 19206–19211; (*f*) Y. Zhou, M. Yang, S. Pang, K. Zhu and N. P. Padture, *J. Am. Chem. Soc.*, 2016, **138**, 5535–5538.
3 G. E. Eperon, S. D. Stranks, C. Menelaou, M. B. Johnston, L. M. Herz and H. J. Snaith, *Energy Environ. Sci.*, 2014, **7**, 982–988.
4 (*a*) J.-W. Lee, D.-H. Kim, H.-S. Kim, S.-W. Seo, S. M. Cho and N.-G. Park, *Adv. Energy Mater.*, 2015, **5**, 1501310; (*b*) C. Yi, J. Luo, S. Meloni, A. Boziki, N. Ashari-Astani, C. Grätzel, S. M. Zakeeruddin, U. Röthlisberger and M. Grätzel, *Energy Environ. Sci.*, 2016, **9**, 656–662.
5 Z. Li, M. Yang, J.-S. Park, S.-H. Wei, J. J. Berry and K. Zhu, *Chem. Mater.*, 2016, **28**, 284–292.
6 C. C. Stoumpos, C. D. Malliaka and M. G. Kanatzidis, *Inorg. Chem.*, 2013, **52**, 9019–9038.
7 M. T. Weller, O. J. Weber, J. M. Frost and A. Walsh, *J. Phys. Chem. Lett.*, 2015, **6**, 3209–3212.
8 N. J. Jeon, J. H. Noh, W. S. Yang, Y. C. Kim, S. Ryu, J. Seo and S. I. Seok, *Nature*, 2015, **517**, 476–480.
9 (*a*) I. Chung, J.-H. Song, J. Im, J. Androulakis, C. D. Malliaka, H. Li, A. J. Freeman, J. T. Kenney and M. G. Kanatzidis, *J. Am. Chem. Soc.*, 2012, **134**, 8579; (*b*) Y. Zhou, H. F. Garces, B. S. Senturk, A. L. Ortiz and N. P. Padture, *Mater. Lett.*, 2013, **110**, 127–129.
10 Y. Zhou, M. Yang, J. Kwun, O. S. Games, Y. Zhao, S. Pang, N. P. Padture and K. Zhu, *Nanoscale*, 2016, **8**, 6265–6270.
11 Q. Han, S.-H. Bae, P. Sun, Y.-T. Hsieh, Y. Yang, Y. S. Rim, H. Zhao, Q. Chen, W. Shi, G. Li and Y. Yang, *Adv. Mater.*, 2016, **28**, 2253–2258.
12 (*a*) Y. Zhou, O. S. Onkar, S. Pang and N. P. Padture, *J. Phys. Chem. Lett.*, 2015, **6**, 4827–4839; (*b*) Y. Zhou, A. L. Vasiliev, W. Wu, M. Yang, S. Pang, K. Zhu and N. P. Padture, *J. Phys. Chem. Lett.*, 2015, **6**, 2292–2297; (*c*) Z. Wang, Y. Zhou, S. Pang, Z. Xiao, J. Zhang, W. Chai, H. Xu, Z. Liu, N. P. Padture and G. Cui, *Chem. Mater.*, 2015, **27**, 7149–7155.
13 C. J. Barbe, F. Arendse, P. Comte, M. Jirousek, F. Lenzmann, V. Shklover and M. Grätzel, *J. Am. Ceram. Soc.*, 1997, **80**, 3157–3171.